

## Ion implant dose dependence of photocarrier radiometry at multiple excitation wavelengths

Derrick Shaughnessy, Bincheng Li, Andreas Mandelis, and Jerias Batista<sup>a)</sup>

Center for Advanced Diffusion-Wave Technologies (CADIFT), Department of Mechanical and Industrial Engineering, University of Toronto, Toronto, Ontario M5S 3G8, Canada

(Received 12 December 2003; accepted 30 April 2004; published online 10 June 2004)

The dependence of the photocarrier radiometric (PCR) signal on ion implant dose in Si is reported. The results show almost entirely monotonic behavior over a large range of industrially relevant fluences ( $1 \times 10^{10}$ – $1 \times 10^{16}$  cm<sup>-2</sup>) for <sup>11</sup>B<sup>+</sup>, <sup>75</sup>As<sup>+</sup>, <sup>31</sup>P<sup>+</sup>, and BF<sub>2</sub><sup>+</sup> implanted in Si wafers at various energies. In addition, the use of excitation sources with a range of absorption coefficients is shown to be very useful in improving the sensitivity of the PCR amplitude to implant dose. © 2004 American Institute of Physics. [DOI: 10.1063/1.1765737]

The implantation of impurity ions has become an important procedure for selective modification of the electrical properties of near surface regions of semiconductor wafers during the manufacturing of various types of semiconductor junctions and devices.<sup>1</sup> Bombardment of the silicon lattice structure by charged ions results in the creation of numerous structural defects. The degree of crystalline damage depends on the mass of the impurity atoms, fluence, energy, as well as the alignment of the ion beam relative to the crystal orientation and has implications on the thermophysical, optical, electrical, and mechanical properties of the near surface region of the material.<sup>1,2</sup> This allows for the application of numerous surface sensitive characterization techniques to be utilized for ion implantation dose uniformity measurements and mapping.<sup>3</sup> In this letter we present the application of photocarrier radiometry (PCR) to ion implantation dose monitoring.

Photocarrier radiometry, a form of modulated room-temperature near-infrared photoluminescence, has recently been introduced as a novel photonic nondestructive diagnostic technique that measures the infrared emission from a sample excited by an intensity modulated super-band-gap optical source.<sup>4</sup> The creation of excess electron-hole pairs results in carrier densities above the intrinsic level and a corresponding harmonic variation of the infrared absorption coefficient. According to Kirchhoff's law, the radiation absorbed by a material in thermal or electronic equilibrium is balanced by the radiation it emits.<sup>4,5</sup> The harmonic IR emissions due to the generated excess carriers are judiciously filtered from any thermal IR (Planck-mediated) emissions resulting from harmonic temperature variations and are monitored with an appropriate spectrally gated detector. The PCR signal is proportional to the depth integral of the carrier density in the sample:<sup>4</sup>

$$P(\omega) \approx F_2(\lambda_1, \lambda_2) \int_0^L \Delta N(z, \omega) dz, \quad (1)$$

where  $L$  is the sample thickness and  $F_2$  is a constant that depends on the spectral bandwidth of the detector and the optical and electrical properties of the sample. A discussion

of the theoretical aspects of PCR can be found in Ref. 4.

The substrates used in this experiment were (100) oriented  $p$ -type silicon wafers ( $675 \mu\text{m} \pm 20 \mu\text{m}$ ,  $7\text{--}8 \Omega \text{cm}$ ) with a thermally grown oxide layer of  $200 \text{ \AA}$ . These wafers were implanted at room temperature at an angle of  $7^\circ$  to suppress channeling with fluences from  $10^{10}$  to  $10^{16}$  cm<sup>-2</sup> with the following species and energy combinations: <sup>11</sup>B<sup>+</sup> (10 keV, 50 keV, 180 keV), <sup>75</sup>As<sup>+</sup> (80 keV, 150 keV), <sup>31</sup>P<sup>+</sup> (30 keV, 80 keV, 285 keV), and BF<sub>2</sub><sup>+</sup> (30 keV, 50 keV).

The experimental apparatus has been described previously.<sup>4</sup> A tunable Ti:sapphire laser was used as an excitation source. The radius of the excitation beam was measured to be approximately  $20 \mu\text{m}$ . The IR emissions from the samples were collected through a pair of reflecting objectives, passed through a spectrally matched filter to eliminate any leakage of the excitation source, and focused onto an InGaAs detector with a bandwidth of  $0.8\text{--}1.8 \mu\text{m}$ .

Modulation frequency scans were performed from 100 Hz to 100 kHz on all of the samples using excitation wavelengths of 710 and 830 nm. In order to make use of the variations in signal amplitude for different excitation wavelengths the laser power was adjusted to achieve constant photon flux across the sample surface. Theoretical reflectance values of 0.337 and 0.327 for 710 and 830 nm, respectively, were calculated from published optical properties of crystalline silicon.<sup>6</sup> Accounting for this variation in reflectance and photon energy, the incident powers used for the experiments were 35.6 and 30 mW at 710 and 830 nm, respectively.

It is well known that the ion implantation process in crystalline Si alters the atomic arrangement and the optical properties of the material. Popescu and Boca<sup>7</sup> have shown a correlation between the refractive index of an ion implanted sample and the degree of disorder in the lattice structure. Prussin *et al.*<sup>8,9</sup> have shown that for the relatively heavy P<sup>+</sup> and As<sup>+</sup> ions implanted in Si at a high energy, there is a dose at which the subsurface amorphous layer grows sufficiently large so that the surface crystalline layer ceases to exist, and that at some higher dose dynamic annealing results in the contraction of the amorphous layer thickness and the reformation of a crystalline or polycrystalline surface layer. The lower degree of damage caused during the B<sup>+</sup> implantation process results in the disappearance of the crystalline surface layer at a dose of approximately  $10^{16}$  cm<sup>-2</sup> at 60 keV com-

<sup>a)</sup>On leave from: Departamento de Física, Universidade Federal do Maranhão, Av. Dos Portugueses, s/n, 65085-580 São Luis, MA, Brazil; electronic mail: jbatista@ufma.br

pared to a dose of approximately  $10^{14}$   $\text{cm}^{-2}$  for  $\text{As}^+$  at energies of 50, 90, and 190 keV.<sup>9</sup> The range of implanted ions can be calculated from theory<sup>10</sup> and is available in tabulated form.<sup>11</sup>

In order to correct for any variations in photon flux into the sample resulting from process dependent changes in the reflectance, the reflectance of all samples was measured at each wavelength and the amplitude normalized using the ratio of the calculated to measured value. Implantation of heavier species resulted in reflectivities increasing from 0.32 to approximately 0.41 at doses of approximately  $10^{14}$   $\text{cm}^{-2}$  and in some instances beginning to decline near  $10^{16}$   $\text{cm}^{-2}$ . The samples implanted with the light  $\text{B}^+$  ions showed only a slight increase in reflectance in the  $10^{15}$ – $10^{16}$   $\text{cm}^{-2}$  range. The increase in reflectance appears to be correlated to the evolution of the multilayer crystalline-amorphous-crystalline structure when one takes into account the higher refractive index of amorphous Si compared to the crystalline form.<sup>7,12,13</sup>

Compromised electronic quality resulting from the destruction of the lattice structure during ion bombardment significantly decreases the lifetime of the photoinjected carriers resulting in a constant amplitude well into the kHz range and a phase essentially independent of dose up to the measured 100 kHz.<sup>4</sup> It should be noted here that the PCR signal is proportional to the integral of the carrier density over the thickness of the wafer [Eq. (1)] and is not a thermal-wave signal. Unlike photothermal signals, the nonthermal nature of the PCR amplitudes yields essentially flat scans (independent of frequency) in the range between 428 Hz and 11.29 kHz (10 data points taken over approximately 6 min). This feature allowed averaging in order to minimize the influence of laser power fluctuations that occurred on a time scale greater than the time required for a single measurement but much less than that required for the entire frequency scan. The resulting amplitudes are presented as a function of fluence in Fig. 1.

Inspection of Figs. 1(a) through Fig. 1(d) shows that the PCR signal dependence on dose can be broken down roughly into four regions with the actual dose defining the transition of each region depending on the mass of the implanted ion. In region I the amplitude decreases rapidly with increasing dose as the degree of damage to the lattice structure increases and electronic integrity of the surface region is compromised resulting in carrier trapping, increased surface recombination velocities, and decreased diffusivities and lifetimes. In region II the electronic sensitivity to dose begins to saturate and the amplitude decreases slightly as the size of the damaged region increases with dose.<sup>8</sup> The production of amorphous phase Si brings the onset of sensitivity to the optical properties in region III resulting in another dose range of rapidly decreasing amplitude as the absorption coefficient increases and results in a greater percentage of the photogenerated carriers being created in a region of compromised electronic integrity. For the more massive  $\text{As}^+$  implants a fourth region is visible as the onset of optical saturation occurs near  $10^{16}$   $\text{cm}^{-2}$  and the sensitivity to dose again experiences a rapid decline. Saturation of the electrical sensitivity prior to the onset of the optical sensitivity is a result of the dependence of the carrier-diffusion-wave on electrical percolation paths and the dependence of the optical properties of the sample on relatively large volumes.<sup>14</sup> A detailed discussion of the PCR signal dependence on dose including quantitative

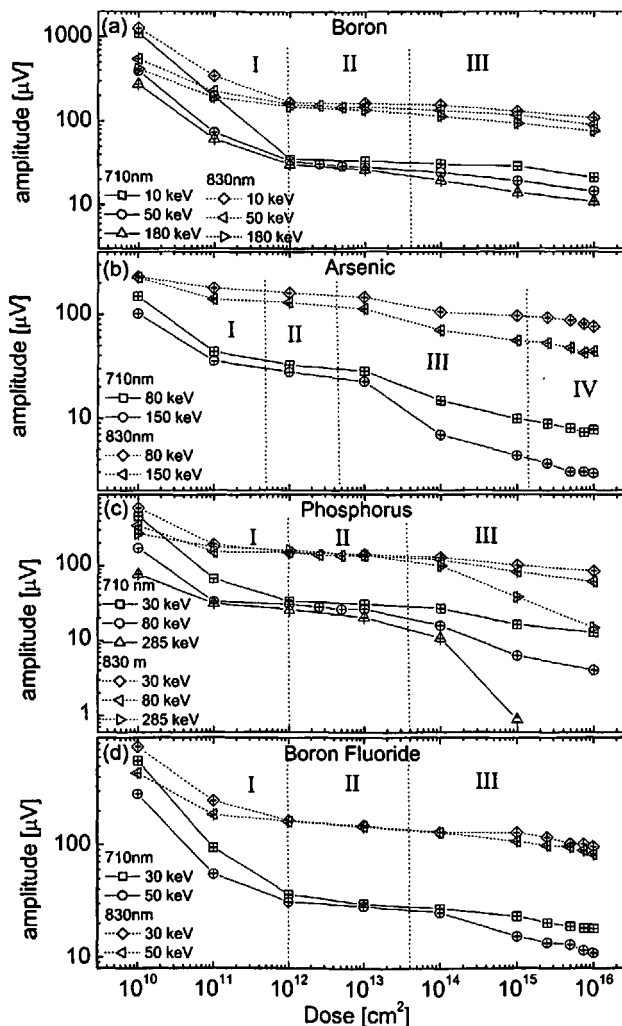


FIG. 1. PCR amplitude versus ion implant dose with 710 nm and 830 nm excitation for: (a)  $^{11}\text{B}^+$ , (b)  $^{75}\text{As}^+$ , (c)  $^{31}\text{P}^+$ , and (d)  $\text{BF}_2^+$ .

modeling will be presented in future papers.<sup>15,16</sup>

A key feature of the results presented in Fig. 1 is the monotonic behavior over a large range of implant dose. The only exceptions for the wafers studied were the  $\text{B}^+$  and  $\text{P}^+$  implanted samples that exhibited slightly nonmonotonic behavior in the  $5 \times 10^{12}$  to  $10^{13}$   $\text{cm}^{-2}$  region at intermediate energy levels and the  $\text{As}^+$  implanted samples that had nonmonotonic behavior above  $5 \times 10^{15}$   $\text{cm}^{-2}$ . This monotonic behavior is an advantage over photothermal techniques such as photomodulated reflectance which exhibit nonmonotonic signals over this dose range due to the competing thermal-wave and carrier-wave components that generate them.<sup>17</sup>

Several other features of note in Fig. 1 are the PCR dependence on energy and on excitation wavelength. In general, the amplitude decreases with implant energy as the depth of the damaged region increases and consumes a greater portion of the photogeneration volume. Similarly, for a given energy, the amplitude decreases with the excitation wavelength as the increasing absorption coefficient results in a photogeneration volume closer to the implanted region. Both of these phenomena are the result of a modification of the weighting of the contributions to the PCR signal from the (damaged) surface region and the bulk of the sample.<sup>18,19</sup> Quantitatively, this amounts to the separation of the depth integral presented in Eq. (1) into one integral over the near-surface region and a second over the remaining thickness of

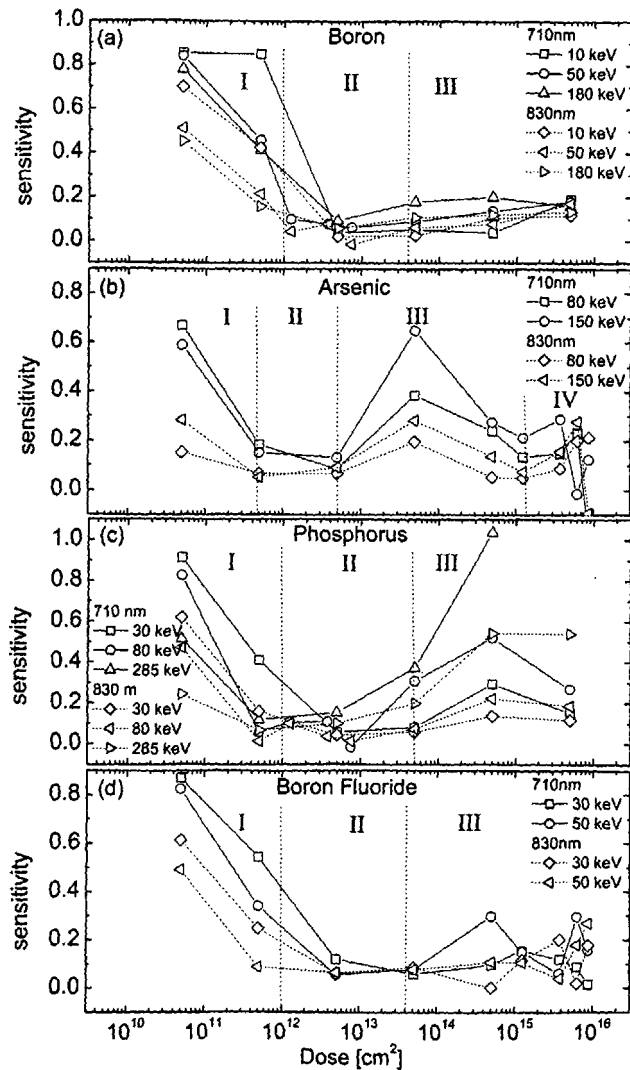


FIG. 2. PCR sensitivity vs ion implant dose with 710 and 830 nm excitation for: (a)  $^{11}\text{B}^+$ , (b)  $^{75}\text{As}^+$ , (c)  $^{31}\text{P}^+$ , and (d)  $\text{BF}_2^+$ .

the wafer with the relative magnitude of each dependent on the number of carriers generated within each region.

Increasing the relative contribution of the surface region to the PCR signal compared to that of the bulk by increasing the absorption coefficient of the excitation source also increases the overall sensitivity of the technique to dose. The total percentage change in signal over the entire range of fluences was larger for 710 nm excitation than for 830 nm for each species and energies. With the exception of the  $\text{P}^+$  implanted sample at 285 keV, which was extremely sensitive to high dose at 710 nm, the ratio of overall sensitivity at 710 nm to that at 830 nm ranged from 1.14 for  $\text{B}^+$  10 keV to 1.78 for  $\text{As}^+$  80 keV. All species except arsenic showed an increase in this sensitivity ratio with implant energy.

The sensitivity of the PCR signal to dose is defined as<sup>20</sup>  $S = [(A_j - A_k)/(A_j + A_k)] / [(D_k - D_j)/(D_j + D_k)]$  where  $A$  is the signal amplitude,  $D$  is the dose, and  $j$  and  $k$  are consecutive data points corresponding to adjacent dose measurements. The sensitivity is presented as a function of fluence in Fig. 2. Decreasing the excitation wavelength resulted in an increased sensitivity for nearly all of the ranges studied with the notable exceptions of the high dose  $\text{As}^+$  implants ( $>5$

$\times 10^{15} \text{ cm}^{-2}$ ) which were nonmonotonic and the high dose  $\text{BF}_2^+$  implants. This increased sensitivity with decreasing excitation wavelength is a result of a greater weighting of the PCR signal on the damaged region of the sample as described above. The change in sensitivity from regions of high dependence on dose to saturation for the electronic and optical effects on the PCR signal, as discussed earlier, is clearly present in Fig. 2. The values presented in Fig. 2 do compare favorably, especially in the low dose region using the shorter excitation wavelength, with photomodulated reflectance results for the same species over the same dose and energy ranges.<sup>21</sup>

The presented experimental results coupled with the optimization of the absorption depth of the excitation source and the potential to improve the signal level through minor modifications of the instrument demonstrate the potential for photocarrier radiometry as an industrially competitive alternative to existing diagnostic techniques for semiconductor ion implantation process control.

The authors wish to acknowledge the continuing support of Materials and Manufacturing Ontario (MMO) and Photo-Thermal Diagnostics, Inc., with a Collaborative Project Contract, and of the Natural Science and Engineering Research Council of Canada (NSERC).

<sup>1</sup>K. A. Pickar, *Applied Solid State Science*, Vol. 5 (Academic, New York, 1975).

<sup>2</sup>G. Carter and W. A. Grant, *Ion Implantation of Semiconductors* (Arnold, London, 1976).

<sup>3</sup>C. B. Yarling, W. A. Keenan, and L. A. Larson, *Nucl. Instrum. Methods Phys. Res. B* **55**, 235 (1991).

<sup>4</sup>A. Mandelis, J. Batista, and D. Shaughnessy, *Phys. Rev. B* **67**, 205208 (2003).

<sup>5</sup>A. Mandelis, *Solid-State Electron.* **42**, 1 (1998).

<sup>6</sup>D. F. Edwards, in *Handbook of Optical Constants of Solids*, edited by E. D. Palik (Academic, New York, 1998).

<sup>7</sup>G. Popescu and I. Boca, *Thin Solid Films* **233**, 207 (1993).

<sup>8</sup>S. Prussin, D. I. Margolese, and R. N. Tauber, *J. Appl. Phys.* **54**, 2316 (1983).

<sup>9</sup>S. Prussin, D. I. Margolese, and R. N. Tauber, *J. Appl. Phys.* **57**, 180 (1985).

<sup>10</sup>J. F. Ziegler, J. P. Biersack, and U. Littmark, *The Stopping and Range of Ions in Solids* (Pergamon, New York, 1996).

<sup>11</sup>J. F. Gibbons, W. S. Johnson, and S. W. Mylorie, *Projected Range Statistics: Semiconductors and Related Materials*, 2nd ed. (Dowden, Hutchinson, & Ross, Stroudsburg, 1975).

<sup>12</sup>B. L. Crowder, R. S. Title, M. H. Brodsky, and G. D. Pettit, *Appl. Phys. Lett.* **16**, 205 (1970).

<sup>13</sup>M. H. Brodsky, R. S. Title, K. Weiser, and G. D. Pettit, *Phys. Rev. B* **1**, 2632 (1970).

<sup>14</sup>C. H. Wilbertz, K. L. Bhatia, W. Krätschmer, and S. Kalbitzer, *Mater. Sci. Eng., B* **2**, 325 (1989).

<sup>15</sup>B. Li, D. Shaughnessy, A. Mandelis, J. Baptista and J. Garcia, *J. Appl. Phys.* (to be published).

<sup>16</sup>B. Li, D. Shaughnessy, A. Mandelis, J. Baptista, and J. Garcia, *J. Appl. Phys.* (to be published).

<sup>17</sup>A. Salmick and J. Opsal, *Rev. Sci. Instrum.* **74**, 545 (2003).

<sup>18</sup>D. Shaughnessy and A. Mandelis, *J. Appl. Phys.* **93**, 5244 (2003).

<sup>19</sup>A. Othonos and C. Christofides, *Nucl. Instrum. Methods Phys. Res. B* **117**, 367 (1996).

<sup>20</sup>D. H. Rosenblatt and J. A. McMillen, *Proceedings of the 11th International Conference on Ion Implantation Technology*, 1997, p. 210.

<sup>21</sup>D. Kamenitsa, P. Lillian, G. Luckman, K. Becker, N. Colvin, M. Rendon, and Z. Bokharey, *2000 International Conf. Ion Implantation Technology*, 2000, p. 674.